Experimental and computational study of the injection of antiprotons into a positron plasma for antihydrogen production

C. Amole, M. D. Ashkezari, M. Baquero-Ruiz, W. Bertsche, E. Butler et al.

Additional information on Phys. Plasmas

Experimental and computational study of the injection of antiprotons into a positron plasma for antihydrogen production

C. Amole,[1] M. D. Ashkezari,[2] M. Baquero-Ruiz,[3] W. Bertsche,[4,5,6] E. Butler,[7,a] A. Capra,[1]
C. L. Cesar,[8] M. Charlton,[4] A. Deller,[4] S. Eriksson,[4] J. Fajans,[3,9] T. Friesen,[10]
M. C. Fujiwara,[11,10] D. R. Gill,[11] A. Gutierrez,[12] J. S. Hangst,[13] W. N. Hardy,[12,14]
M. E. Hayden,[2] C. A. Isaac,[4] S. Jonsell,[15] L. Kurchaninov,[11] A. Little,[3] N. Madsen,[4]
J. T. K. McKenna,[16] S. Menary,[1] S. C. Napoli,[4] K. Olchanski,[11] A. Olin,[11,17] P. Pusa,[16]
C. Ø. Rasmussen,[13] F. Robicheaux,[18] E. Sarid,[19] C. R. Shields,[4] D. M. Silveira,[8] C. So,[3]
S. Stracka,[11] R. I. Thompson,[10] D. P. van der Werf,[4] J. S. Wurtele,[3,9] A. Zhmoginov,[3]
(ALPHA collaboration), and L. Friedland[20]

[1]*Department of Physics and Astronomy, York University, Toronto, M3J 1P3 Ontario, Canada*
[2]*Department of Physics, Simon Fraser University, Burnaby, V5A 1S6 British Columbia, Canada*
[3]*Department of Physics, University of California, Berkeley, California 94720, USA*
[4]*Department of Physics, College of Science, Swansea University, SA2 8PP Swansea, United Kingdom*
[5]*School of Physics and Astronomy, University of Manchester, M13 9PL Manchester, United Kingdom*
[6]*Daresbury Laboratory, The Cockcroft Institute, WA4 4AD Warrington, United Kingdom*
[7]*Physics Department, CERN, CH-1211 Geneva 23, Switzerland*
[8]*Instituto de Física, Universidade Federal do Rio de Janeiro, Rio de Janeiro 21941, Brazil*
[9]*Lawrence Berkeley National Laboratory, Berkeley, California 94720, USA*
[10]*Department of Physics and Astronomy, University of Calgary, Calgary, T2N 1N4 Alberta, Canada*
[11]*TRIUMF, 4004 Wesbrook Mall, Vancouver, V6T 2A3 British Columbia, Canada*
[12]*Department of Physics and Astronomy, University of British Columbia, Vancouver, V6T 1Z1 British Columbia, Canada*
[13]*Department of Physics and Astronomy, Aarhus University, DK-8000 Aarhus C, Denmark*
[14]*Canadian Institute of Advanced Research, Toronto, M5G 1Z8 Ontario, Canada*
[15]*Department of Physics, Stockholm University, SE-10691 Stockholm, Sweden*
[16]*Department of Physics, University of Liverpool, L69 7ZE Liverpool, United Kingdom*
[17]*Department of Physics and Astronomy, University of Victoria, Victoria, V8W 3P6 British Columbia, Canada*
[18]*Department of Physics, Auburn University, Auburn, Alabama 36849, USA*
[19]*Department of Physics, Nuclear Research Center Negev, Beer Sheva, Israel*
[20]*Racah Institute of Physics, The Hebrew University, Jerusalem, Israel*

One of the goals of synthesizing and trapping antihydrogen is to study the validity of charge–parity–time symmetry through precision spectroscopy on the anti-atoms, but the trapping yield achieved in recent experiments must be significantly improved before this can be realized. Antihydrogen atoms are commonly produced by mixing antiprotons and positrons stored in a nested Penning-Malmberg trap, which was achieved in ALPHA by an autoresonant excitation of the antiprotons, injecting them into the positron plasma. In this work, a hybrid numerical model is developed to simulate antiproton and positron dynamics during the mixing process. The simulation is benchmarked against other numerical and analytic models, as well as experimental measurements. The autoresonant injection scheme and an alternative scheme are compared numerically over a range of plasma parameters which can be reached in current and upcoming antihydrogen experiments, and the latter scheme is seen to offer significant improvement in trapping yield as the number of available antiprotons increases. © *2013 AIP Publishing LLC.* [http://dx.doi.org/10.1063/1.4801067]

I. INTRODUCTION

The antihydrogen ($\bar{\text{H}}$) atom is the only neutral antimatter system that has been synthesized,[1,2] trapped,[3,4] and held for long periods of time.[5] The goal of these developments is to establish the methods and physical apparatus needed for the precision measurement of the physical properties of antihydrogen, which may shed light on the baryon asymmetry of our universe, one of the great unresolved problems of physics. The validity of charge–parity–time (CPT) symmetry can also be tested by comparing hydrogen and antihydrogen spectrums. The ALPHA collaboration's recent observation of a resonant interaction of antihydrogen atoms with microwave[6] served as a proof of concept for measuring the physical properties of trapped antihydrogen, but the precision achieved ($O(10^{-3})$) is hampered by the low number of trapped antihydrogen atoms (~ 1) per attempt and cannot yet be compared to that of hydrogen spectroscopy.[7]

To undertake measurements on antihydrogen atoms with enough precision to yield insight into CPT symmetry (e.g., laser and microwave spectroscopy, charge neutrality, and gravity measurement), a much higher trapping rate is essential to improve statistics, overcome systematics and

---

a)Current address: Centre for Cold Matter, Imperial College, SW7 2BW London, United Kingdom.

backgrounds, and ensure stability by reducing the number of runs required to accumulate data. Some experimental techniques to improve precision and stability, like laser cooling and optical confinement, also require a much greater number of trapped antihydrogen. It is, therefore, necessary to understand the possibilities and limits of antihydrogen synthesis schemes in order to select the best strategy and maximize the number of trappable antihydrogen atoms.

The core of the ALPHA apparatus consists of a stack of cylindrical electrodes placed in the bore of a superconducting solenoidal magnet, forming a highly configurable Penning–Malmberg trap[8] for manipulating electrons (e^-), positrons (e^+), and antiprotons ($\bar{p}$). The 5.3 MeV antiproton bunch delivered by the Antiproton Decelerator (AD) at CERN is passed through a degrading foil and subject to a series of cooling manipulations which reduce its energy by 8 orders of magnitude to ∼250 K. Concurrently, positrons are delivered by a Surko-type accumulator[9] from the other end of the electrode stack and cooled. Both species are subject to further manipulations to tailor their sizes and numbers. The two species are then transferred to the central region of the electrode stack and stored adjacent to each other in a nested well. A magnetic minimum trap superimposed on the center of the electrode stack is then energized before the antiprotons are excited from their well such that their orbits cross into the adjacent well occupied by the positrons. Antihydrogen atoms are assumed to form through three-body recombination[10] between the positrons and antiprotons, and ground state antihydrogen atoms with a kinetic energy (KE) less than ∼0.54 K are confined by their magnetic moment. A detailed description of the experiment is given by Andresen *et al.*[11]

In our recent studies,[5,6] only ∼1 of the ∼10 000 synthesized antihydrogen atoms remains in the neutral trap in each 15 min experimental run, with the rest escaping and annihilating on the physical wall after formation. Useful physics can be obtained from such a low trapping rate because of the hour-long antiproton and positron lifetime achieved in the apparatus, and because the silicon vertex detector provides spatially and temporally resolved antihydrogen detection down to a single-atom sensitivity.[12] Nonetheless, achieving the precision necessary to resolve CPT symmetry or the bayron asymmetry problem requires increased trapping rate and a colder antihydrogen atom distribution.

Whether an antihydrogen atom can be magnetically trapped depends on its KE and its spin state. The KE of the antihydrogen atoms is almost exclusively determined by that of the antiprotons immediately before recombination (since the positrons are much lighter). The number of antihydrogen atoms trapped thus depends on the energy at which the antiprotons are injected into the positron plasma, as well as a number of factors:

1. The injected antiprotons equilibrate with the positrons through Coulomb collisions.
2. The positrons, whose velocity distribution is perturbed by the injected antiprotons, re-equilibrate with the background radiation.
3. The antiprotons recombine with positrons in a three-body recombination process, which cross-section is a function

of their relative velocity. At the moment of recombination, the KE of the antiprotons is "frozen" into that of the antihydrogen atoms.

4. The antihydrogen atoms formed are initially in a high quantum state, making them easier to confine, since they are more likely to possess a higher magnetic moment. The anti-atoms subsequently reach lower quantum states through radiative cascade, or become field-ionized in the process.

Antiprotons initially sit in a electrostatic well adjacent to the positrons and are injected through an excitation of their axial oscillation such that their orbits cross into the positron plasma. The optimal excitation should allow the majority of the antiprotons to gain just enough energy to cross into the positron plasma, ensuring that the antiprotons start their equilibration with the positrons at the minimum KE. This was achieved in the recent ALPHA studies[3,6] by autoresonantly exciting the axial oscillation of the antiproton bunch. A weak, frequency-chirped, oscillating signal is generated by an arbitrary waveform generator and fed through a high-pass filter to one of the electrodes near the antiproton bunch (which also has a non-zero DC background forming part of the nested well; see Fig. 1), creating an additional oscillating force across the antiproton bunch. The antiprotons automatically become phase-locked to the perturbation under specific conditions and oscillate with increasing amplitude. Phase lock between the antiprotons and the perturbation is ultimately lost when injection occurs, and the mean
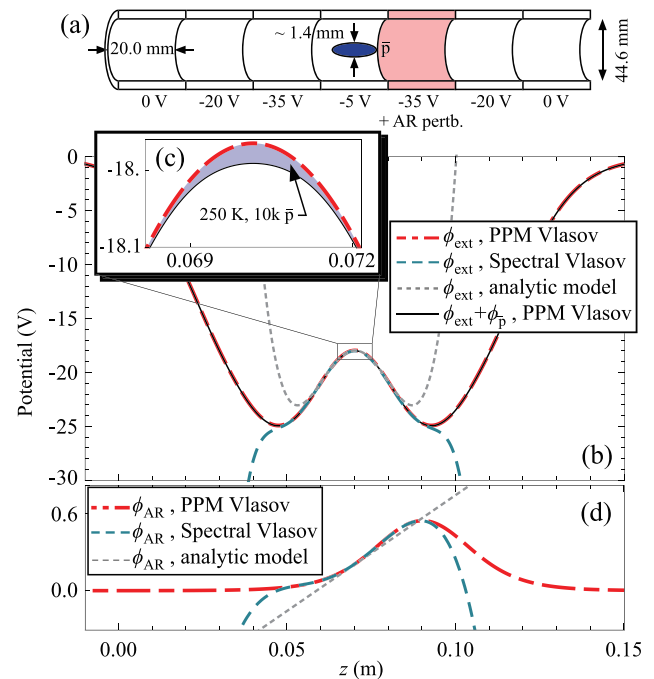

FIG. 1. Potentials and geometry for measuring the AR excitation of an antiproton bunch. (a) The physical setup, with the electrode marked pink connected to the AR signal. (b) The external potential created by the electrodes at $r = 0$. (c) A close-up of b, emphasizing the effect of various antiproton space charges. (d) The perturbation created at $r = 0$ when 1 V is applied to the AR electrode. The potentials used in the PPM Vlasov model are deduced by solving the 2D Poisson equation with physically accurate boundary conditions. Those in the spectral Vlasov solver are analytic fits up to z^6. The external potential ϕ_{ext} in the analytic model fits up to z^4, and the perturbation ϕ_{AR} to z^1.

antiproton energy stops increasing. This self-arresting nature of autoresonant (AR) excitation means it is robust against shot-to-shot variation in antiproton and positron numbers. Without this mechanism, it is likely that the fluctuations would misalign the potential between antiprotons and positrons during injection by several percent. Given that the nested well potential is ~5 V, and the potential created by the positron space charge is ~2 V, a 5% misalignment gives the antiprotons a kick of $O(1000\,\mathrm{K})$, which would almost certainly eliminate any chance of producing antihydrogen atoms trappable in the 0.54 K-deep neutral trap.

This paper presents the first detailed study of the injection process by simulating the antiproton and positron dynamics during manipulations of the nested Penning-Malmberg trap. In Sec. III, a numerical model is developed, in which the antiproton bunch is modeled dynamically through the Vlasov–Poisson equation, and the positron plasma quasi-statically through the Poisson–Boltzmann equation. The model is benchmarked against other numerical and analytic models in Sec. IV and compared with experimental measurements in Sec. V. The effectiveness of the AR injection technique is studied in Sec. VI across a range of antiproton parameters that can be realized in current and upcoming antihydrogen experiments, and a novel technique is proposed in Sec. VII, which may offer significant improvement to antihydrogen yield when an intense cold antiproton bunch is used.

II. BASIC THEORY OF AUTORESONANT EXCITATION

AR excitation has been applied to, and observed in, a wide variety of systems.[13] The principle of AR excitation is most transparent in the case of a single particle in an anharmonic well. AR excitation in this case only works when there is a monotonic relation between the amplitude and frequency of an oscillator, and for specificity it is assumed to be monotonically decreasing. A fixed frequency perturbation at linear resonance (ω_0) results in a limited excitation since, as the particle is excited, its oscillation frequency changes with amplitude and consequently loses phase lock with the drive. An AR perturbation instead starts at a frequency above ω_0 and is chirped towards a lower frequency. As the frequency passes through ω_0, the particle becomes phase-locked to the perturbation, provided certain conditions are satisfied. The amplitude of the oscillator motion changes such that its frequency automatically matches that of the perturbation. Fajans and Friedland[14] gave an analytic treatment of the AR excitation process for an oscillator with an equation of motion of

$$\ddot{z} + \omega_0^2\left(1 - \frac{4}{3}\beta z^2\right)z = \epsilon\cos\left(\theta_D(t)\right) = \epsilon\,\mathrm{Re}\left(e^{i\theta_D(t)}\right), \quad (1)$$

and derived the conditions that must be met in order for phase-locking to occur. Here, ϵ denotes the drive amplitude, $\theta_D(t) = \omega_0 t - \alpha t^2/2$ the drive phase angle, $-\alpha$ the rate of change of the drive frequency, or chirp rate, and β the nonlinearity of the oscillator. The motion starts at a large negative t with $z = \dot{z} = 0$, and the perturbation passes through the

linear frequency at $t = 0$. The derivation starts by separating the fast and slow motion of the oscillator:

$$z(t) = \mathrm{Re}\left(a(t)e^{i\theta_P(t)}\right), \quad (2)$$

where $a(t)$ is the slowly varying time-dependent oscillator amplitude and $\theta_P(t)$ is the phase. The amplitude $a(t)$ and phase difference $\delta(t) \equiv \theta_P - \theta_D$ vary on a timescale $\gg 1/\omega_0$.

For t near zero, and ignoring higher harmonics, substituting Eq. (2) into Eq. (1) gives

$$\dot{I} = -\frac{\epsilon}{\sqrt{2}\omega_0}\sqrt{I}\sin(\delta), \quad (3)$$

$$\dot{\delta} = \alpha t - \omega_0\beta I - \frac{\epsilon}{2\sqrt{2}\omega_0}\frac{1}{\sqrt{I}}\cos(\delta), \quad (4)$$

where $I(t) \equiv a^2(t)/2$. By expanding $\delta(t)$ around π, the locked, stable phase, one can show[14] that for phase-locking to occur,

$$\epsilon > \epsilon_{\mathrm{cr}} \equiv 2\sqrt{2}\sqrt{\frac{\omega_0}{\beta}}\left(\frac{\alpha}{3}\right)^{3/4} \quad (5)$$

must be satisfied.

Generalizing the single particle dynamics above to the excitation of an antiproton bunch in a nested Penning–Malmberg trap is not trivial. Ignoring collective response, a test particle alone will not exhibit AR excitation since the net electrostatic well (including the antiproton self-field) does not have a monotonic relationship between amplitude and frequency. Barth *et al.*[15] presented theoretical results showing that the self-field causes the plasma to remain coherent during an AR perturbation. The experimental observation of AR phase-locking and excitation in the collective regime was first presented by Andresen *et al.*[16]

III. NUMERICAL MODEL

The AR injection process is highly nonlinear and involves the interaction of two species moving on very different timescales, which makes its numerical simulation non-trivial. Some simplification is afforded by the presence of a strong (1 T) solenoidal magnetic field. The process of interest—the excitation of the axial oscillation of antiprotons by an external perturbation—happens on the timescale of the antiproton axial bounce period, which, according to Table I, is much shorter than the mean free time between collisions of antiprotons. Indeed, the antiproton mean free time is comparable to the duration of an entire AR chirp in a typical simulation (~1 ms). The antiproton bunch can therefore be regarded as approximately collisionless. The antiproton cyclotron radius is much smaller than the radial size of the plasma, and its cyclotron motion has a much shorter period than its axial bounce motion, meaning that the antiprotons move at well-defined radii, little radial transport occurs, and the parallel and perpendicular motions are well separated. The effective antiproton–positron collision frequency is coincidentally similar to that of antiproton–antiproton

TABLE I. Typical plasma conditions and parameters just before injection manipulations. The uncertainties in particle numbers refer to the shot-to-shot fluctuation of the species. The plasma dimensions are defined by the region enclosed by the equi-density contour in *r*–*z* space that encloses 90% of the total material, and the density is defined by the average therein. The Debye lengths and plasma oscillation periods are derived from this average density. The mean free time is the mean time between effective collisions estimated from the non-magnetized Coulomb collision model.

	Antiproton	Positron
Number	$16,000 \pm 5\%$	$3 \times 10^6 \pm 5\%$
Density (m^{-3})	3×10^{12}	7×10^{13}
Temperature (K)	250	40
Self-field (V)	0.05	2
Length (mm)	4	23
Radius (mm)	0.7	0.9
Debye length (mm)	0.6	0.05
Cyclotron radius (mm)	0.02	2×10^{-4}
Mean free time (μs)	700	0.8
$E \times B$ drift period (μs)	70	10
Axial bounce period (μs)	3	0.3
Plasma oscillation period (μs)	3	0.01
Cyclotron period (μs)	0.07	4×10^{-5}

collisions for the typical plasma parameters shown in Table I and is therefore neglected. The antiproton bunch is thus regarded as a collection of cylindrical shells, with their axes, defined as the *z*-direction, lying parallel to the magnetic field of the Penning trap.[17] The antiprotons (or more accurately, their guiding centers) in each shell move only in the *z*-direction as free particles influenced by the *z*-component of the total electrostatic field, and their motion is described by a (z, v_z) phase space distribution which evolves according to the Vlasov equation. Particles in different tubes are coupled through the antiproton self-field, which is found by solving the Poisson equation using the antiproton charge density in each shell.

The Vlasov equation governing the evolution of each cylindrical shell is solved numerically using operator splitting. The individual advection operators are discretized using the flux balance method[18] together with the piecewise parabolic reconstruction method[19] (PPM). The antiproton self-field is solved for using a numerical Green's function.

The positron plasma, on the other hand, is highly collisional on the antiproton axial bounce timescale. It is effectively Debye-shielded, and each positron executes about ten axial bounces in the time an antiproton has undergone one. It is observed experimentally that the positron radial profile does not change appreciably after the AR perturbation. The positron plasma is thus approximately in a self–consistent axial thermal equilibrium with the total electrostatic potential; i.e., the positron plasma adjusts itself axially along field lines to satisfy the Poisson–Boltzmann equation at all times, but the radial profile of the positron plasma remains unchanged.

The Poisson–Boltzmann equation for the positron plasma is solved numerically in the zero–temperature limit by the so–called water–bag model. The water-bag solver takes an experimentally measured positron radial profile and

voltages on the electrodes as input and solves for the axial profile that gives a perfect Debye shielding of the *z*-component of the total electric field within the profile. This total field is then used in the acceleration term in the antiproton Vlasov equation. In cases where the applied voltage is strong enough that the positron plasma starts to escape, a more sophisticated Vlasov-based solver, which models the evaporative escape and radial redistribution process and solves for the self-consistent distribution of the remaining population, is used.

The effects of the octupole and mirror fields that comprise the neutral trap are ignored in this model, since their effect on particle orbits is small. At 1 mm from the axis, the octupole field is $O(10^{-4}\,\text{T})$, superimposed on the background solenoidal field of 1 T. Within the axial extent of the possible orbits of either species, the mirror trapping force is equivalent to a 0.002 V deep well for particles with a perpendicular energy of 250 K, which is superimposed on the $\sim$5 V deep electrostatic well. The model chiefly predicts the axial (longitudinal) energies of injected antiprotons, ignores $\mathbf{E} \times \mathbf{B}$ rotation and assumes the perpendicular degrees of freedom were well-separated and the energies in these degrees of freedom remain unchanged throughout the manipulations.

IV. COMPARISONS WITH NUMERICAL AND ANALYTIC MODELS

In this section, the PPM Vlasov model is compared with (1) the analytic model (Eqs. (3)–(5)), (2) a leap-frog single particle pusher that neglects the self-field of the antiproton bunch (treats it as a single particle), but evolves it under the same positron, vacuum and AR perturbation fields as in the PPM Vlasov model, and (3) a 1D, single-shell, collisionless spectral Vlasov–Poisson solver used by Barth *et al.*,[15] which solves a 1D Poisson equation with an idealized cutoff representing radial variation.

A. Time-resolved AR excitation

The different models are applied to the AR excitation of a 250 K, 10 000 antiproton bunch with a radius of $\sim$0.7 mm. The particles are confined by an anharmonic electrostatic well with a linear bounce frequency of 412.7 kHz as shown in Fig. 1. The antiproton bunch is excited by an AR perturbation applied to an electrode to the right of the bunch. The perturbation frequency changes linearly from 420 kHz to 200 kHz at a chirp rate of −200 MHz/s, and an amplitude of 0.14 V. A 10–period transition is present before the start of the chirp, where the perturbation amplitude is linearly increased from 0 to its full amplitude, at the starting frequency. A similar transition is present at the end of the chirp. A wait time of 20 periods (measured in terms of the stopping frequency, during which no perturbation is applied) is present before the simulation is terminated. The results from the different models are displayed in Fig. 2, showing similar behavior between the models, in terms of both the energy and the phase of the antiproton bunch. The analytic model prediction shows a slightly higher excitation at later times since it includes only the 4th order non-linearity of the
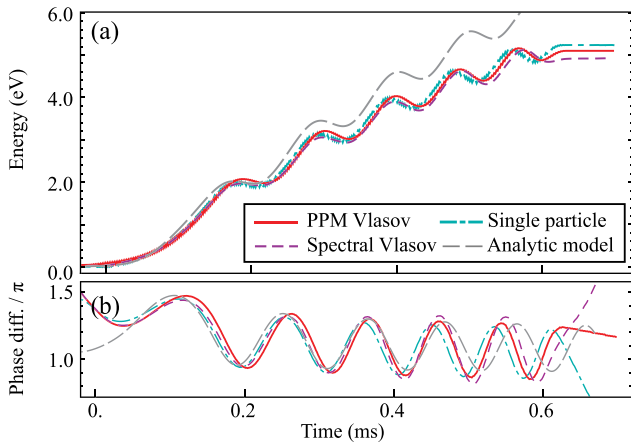
FIG. 2. Time evolution of (a) the energy and (b) phase angle of the antiproton distribution, as predicted by different numerical and analytic models. The phase difference is defined as $\theta_P - \theta_D$, where θ_P is the phase angle of the center of charge of the distribution, and θ_D the phase angle of the AR perturbation.

confining well, while the other models use a more accurate solution of the physical potential.

B. Perturbation amplitude threshold for pickup

In Fig. 3, the analytic prediction for the critical drive amplitude ϵ_{cr} (Eq. (5)) is compared with the single particle model and the PPM Vlasov model. The set up is identical to that shown in Fig. 1, with a 250 K, 10 000 antiproton bunch subjected to different AR perturbations. These perturbations start from 420 kHz with the 10-period ramp-up, and end at 360 kHz with the 10-period ramp-down, but with various amplitudes and the chirp rates. At each chirp rate on the horizontal axis of Fig. 3, multiple simulations with different drive amplitudes are executed, and a sudden jump in the final averaged antiproton energy is observed when the drive amplitude exceeds the critical value. This critical drive amplitude is plotted in the vertical axis of Fig. 3, together with the analytical prediction. Good agreement between the models is again observed.

V. COMPARISONS WITH EXPERIMENT

The results of experimental runs are compared with predictions of the PPM Vlasov model and the single particle
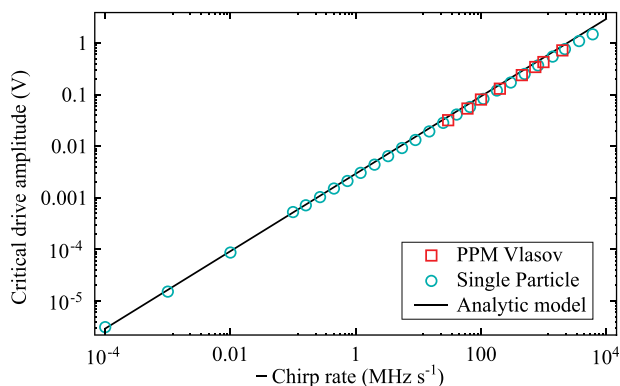

FIG. 3. Critical perturbation amplitude for varying chirp rates. The prediction of the analytic model and the results from the single particle and PPM Vlasov model are compared.

model. In the first comparison, an antiproton bunch is subjected to AR perturbations in an anharmonic well without neighboring positrons, and the resultant antiproton axial energy gain is analyzed. In the second comparison, an antiproton bunch is subjected to AR perturbations next to a positron plasma. Some fraction of the antiprotons obtains sufficient energy to enter the positron plasma, and a smaller fraction goes on to form antihydrogen atoms. The distribution of the KE of the injected antiprotons predicted by simulation is compared with the number of antihydrogen atoms as measured from experiment.

A. Final antiproton energy distribution versus drive amplitude and stopping frequency

A 250 K, ~4000 antiproton bunch is prepared in the anharmonic well shown in Fig. 1, which has a linear frequency of 412.7 kHz. The particles are subjected to various AR perturbations, all of which start from 420 kHz, have a chirp rate of −200 MHz/s and include the 10-period ramp-up and ramp-down. In the first series of runs, the stopping frequency is fixed at 360 kHz, and the drive amplitude varies between 0 V and 0.161 V. In the second series, the drive amplitude is fixed at 0.15 V and the stopping frequency varies between 355 kHz and 390 kHz. From the simulations, the final energy of the antiprotons post-perturbation can be derived from the final phase space distributions/single particle states straight-forwardly. Experimentally, the final energy of the antiproton bunch is measured by lowering one side of the confining potential in 10 ms, which is much slower than the $O(10 \mu s)$ axial bounce period. Those antiprotons with the highest energy escape first, followed by the lower energy population, and they annihilate on the end of the trap. The time-dependent annihilation signal is registered by a scintillator detector. Since the axial adiabatic invariant $J = \oint m_{\bar{p}} v_z \, dz$, where $m_{\bar{p}}$ is the antiproton mass, is approximately conserved during the slow lowering of the confining potential, the one-to-one correspondence between energy in the well and escape time is known. The annihilation signal as a function of time is thus mapped to a distribution as a function of energy in the well.[20] The final energies obtained from the models and the experiment are compared in Fig. 4. The centers of charge of the bunch predicted by the models agree well with experimental measurements, but the PPM Vlasov model predicts a somewhat broader energy distribution than observed in experiment.

Note that the experimental data in Fig. 4 have been fitted to correct for experimental systematics. (i) There is a time synchronization mismatch between the voltage controller for the electrodes and the silicon vertex detector, expected to be within 0.1 ms, introducing a possible offset between the escape time reported by the detector and the actual escape time with respect to the voltage changes being made on the electrodes during a dump. This is accounted for by a time shift of the detector signal such that the detector count from the 0 V drive amplitude experiment in Fig. 4(b) corresponds to an average energy in well of 0 eV. This time offset is then fixed for all other experimental measurements of energy distributions. (ii) The experimental drive amplitude quoted
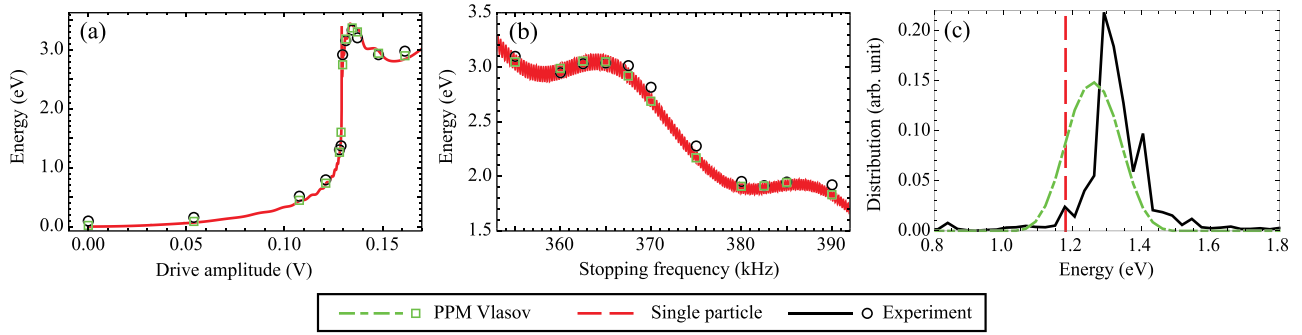
FIG. 4. The final energy of an antiproton bunch after various AR perturbations, as measured in the experiment and predicted by the single particle and the PPM Vlasov models. (a) The final antiproton energy after AR perturbations of various amplitudes and a fixed stopping frequency of 360 kHz. (b) The final antiproton energy after AR perturbations of various stopping frequencies and a fixed amplitude of 0.15 V. (c) The energy distribution of an antiproton bunch after a typical AR perturbation in a—the delta function for the single particle result indicates the inability of the model to simulate a distribution. The experimental data have been corrected for systematics—see main text.

hitherto is the amplitude on the electrode, which is 0.54 times the amplitude at the waveform generator, due to the wiring impedance between the generator and the electrodes. This conversion factor is derived by fitting the horizontal position of the jump in Fig. 4(a) between the experiment and the simulation. This factor is then used in the analysis of all other experimental runs.

B. Injection ratio versus stopping frequency

Figure 5 shows the experimental setup injecting antiprotons into a positron plasma. A 250 K, 16 000 antiproton bunch is placed in a nested well next to a 40 K, 3×10^6 positron plasma, and subjected to an AR perturbation. The antiproton well has a linear frequency of 297.4 kHz, and the perturbation starts at 325 kHz with a 10-period ramp-up to an amplitude of 0.08 V. It is then chirped down to 250 kHz at -120 MHz/s, and ends with a 10-period ramp-down. A fraction of the antiprotons gain enough energy to enter the positron plasma. Due to Debye shielding, the total potential

within the positron plasma is a constant (in z), and therefore each of the injected antiprotons moves across the positron plasma at a constant speed. The simulated distribution of the axial KE of the injected antiprotons as they travel through the positron plasma after the AR perturbation is plotted in Fig. 6(a), together with several phase space snapshots of the antiproton distribution at various times during the AR perturbation in Fig. 6(b).
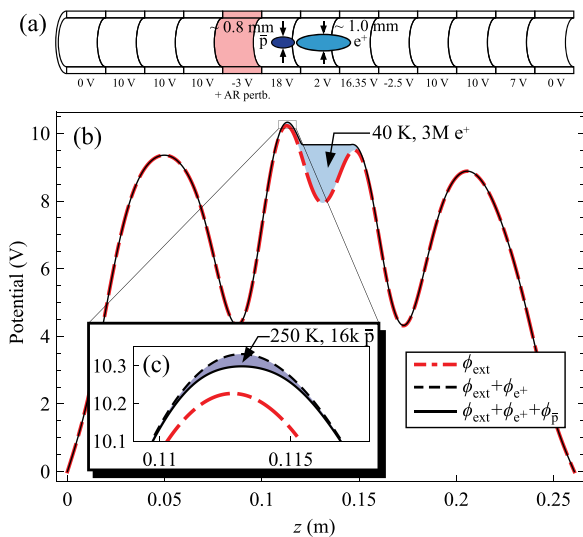

FIG. 5. Potentials and geometry for injecting antiprotons into a positron plasma. (a) The physical setup of the experiment, with the pink electrode connected to the AR signal generator. (b) The external potential created by the electrodes at $r = 0$, and the effect of the positron space charge. (c) A close-up of b, showing the effect of the antiproton space charge.
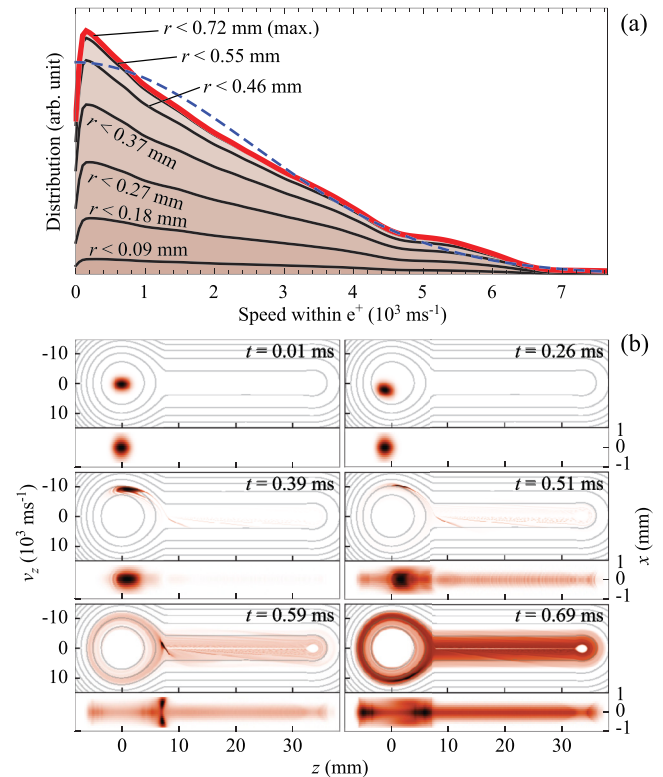

FIG. 6. (a) The simulated distribution in speed of injected antiprotons as they travel across the positron plasma, conditioned on the radius. The blue dotted curve shows a reference thermal distribution of antiprotons at 800 K, which has the same area under the curve as the $r < 0.72$ mm curve. The total number of injected antiproton is 7400 (out of the 16000 initial antiprotons). (b) Simulated antiproton distributions at various t during an AR perturbation. The AR chirp starts at $t = 0$. The contours are lines of constant total energy, and increase by 0.25 eV (2900 K) per contour. At each time, the (z, v_z) phase space at $r = 0$ is displayed, together with the (x, z) charge density.

In the experiment, the KE distribution of the injected antiprotons cannot be measured directly. Instead they cool by collisions with positrons, and some go on to form antihydrogen atoms. Most of the antihydrogen atoms are not confined by the magnetic minimum trap. They drift and eventually annihilate on contact with the electrode wall. The pion tracks from antiproton annihilations are reconstructed from the silicon vertex detector, and the total number of annihilations within a 1 s window after the perturbation is deduced from the detector records. The number of annihilations, divided by the number of antiprotons present before the AR perturbation (estimated by the intensity of the AD beam on each run), is plotted in black in Fig. 7(c), against the stopping frequencies used in various experiments. This ratio indicates the fraction of antiprotons that enters the positron plasma and successfully forms antihydrogen atoms. Figures 7(a) and 7(b) show the simulated fraction of antiprotons which successfully injects and has a KE or radius below various values. For instance, the "KE <100 K" curve in Fig. 7(a) plots the fraction of antiprotons, out of the original 16 000, that successfully enters the positron plasma and travels across it with a KE below 100 K as a function of the AR stopping frequency. Qualitatively, the simulation shows that a chirp stopping below ~290 kHz is necessary for injection. The injected fraction increases as increasingly long chirps are used, but the fraction injected at lower KE (<100 K) slowly saturates when the stopping frequency is below

~240 kHz. The simulation also shows that antiprotons at smaller radii are injected earlier, while those at the outer radii require a longer chirp to reach injection. It is also observed that stopping frequencies much lower than 200 kHz (not shown in Fig. 6) causes the KE distribution of the injected antiprotons to broaden, which is expected since the perturbation, having no frequency relation to the bounce orbits of the injected population, only acts as a heating signal. The number of antihydrogen atoms formed, as measured in the experiment, increases with the length of the AR perturbation, before saturating at a stopping frequency of ~250 kHz (see Fig. 7(c)). This roughly agrees with the simulation. However, a detailed model of antiproton–positron collisional cooling and recombination is necessary to predict the number of antihydrogen atoms formed from the r–z–v_z distribution of injected antiprotons produced from the simulation, which is beyond the scope of this paper.

VI. INJECTION LIMITS

The main adjustable parameters of an antihydrogen production scheme via AR excitation in a nested Penning–Malmberg trap are the numbers, radial sizes and temperatures of the positron plasma and antiproton bunch, as well as the ending frequency, chirp rate and amplitude of the AR perturbation. To maximize the production of trappable antihydrogen atoms, it is instructive to know which of the parameters the antihydrogen yield is most sensitive to, and what limit these parameters pose. Within the confines of the PPM Vlasov model, one can predict the KE distribution of injected antiprotons as a function of the initial antiproton parameters; the results are relatively insensitive to positron parameters since the positron plasma is assumed to evolve according to the quasi-static water-bag model. The dependence of trappable antihydrogen yield on positron parameters enters through equilibration and recombination, which is beyond the scope of the PPM Vlasov model. Still, some qualitative assumptions can be made to connect the injected antiproton KE distribution to the trapped antihydrogen yield. We assume the trappable antihydrogen atoms come mainly from the low-KE portion of the injected antiprotons (defined as <500 K; other definitions yield similar results), since the portion with significantly higher KE would have a small recombination cross-section with the positrons.[10,21] At best, these high-KE antiprotons have no impact on the number of trappable antihydrogen atoms produced. At worst they lead to the heating of the positron plasma and delay recombination, which leaves time for the low-KE antiprotons to equilibrate with the relatively hot positrons, thus reducing the antihydrogen yield.

The impact these antiproton and AR parameters have on the fraction of antiprotons injected at below 500 K is shown in Fig. 8. Different antiproton bunches with various initial numbers and temperatures are fed into the model in the configuration shown in Fig. 5. At each initial number and temperature, various AR perturbations are applied. The optimal stopping frequency and perturbation strength, defined as that which yields the highest fraction of antiprotons injected with KE <500 K, are identified. The corresponding fraction of
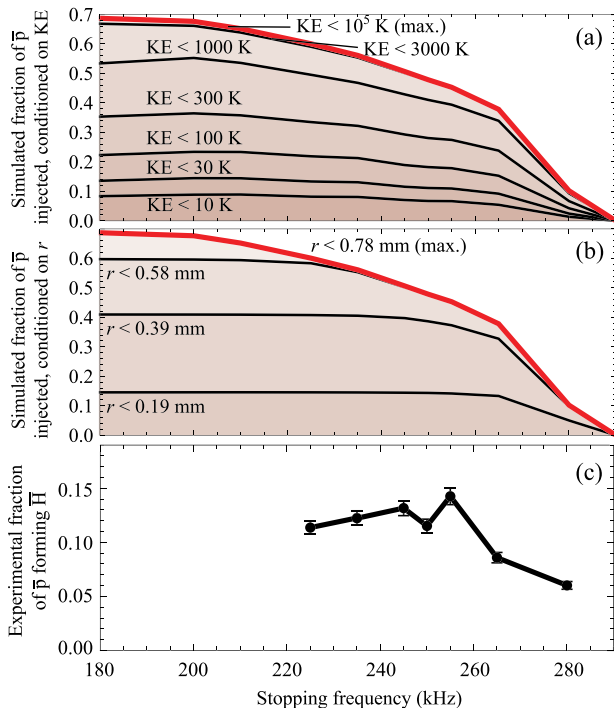

FIG. 7. (a) The simulated fraction of antiprotons injected into the positron plasma conditioned on their injected KE, using AR perturbations of various stopping frequencies. (b) Same as a, except the curves are conditioned on the radius. (c) The number of antiprotons from experiment that successfully inject into the positron plasma and form antihydrogen atoms, divided by the estimated initial number of antiprotons, at various stopping frequencies. The error bars indicate the statistical error of the experimental measurement, and do not include the detector calibration uncertainty ($\sim\pm21\%$) which is systematic to all the data points.
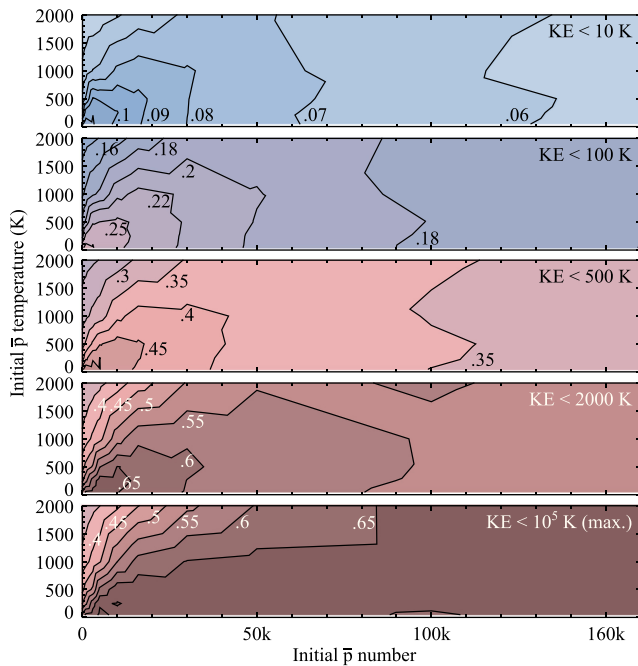
FIG. 8. Contours showing the fraction of antiprotons injected by an AR perturbation into the positron plasma with KE below the indicated value on each subfigure, as a function of the initial antiproton number and temperature. Each antiproton bunch with a specific initial number and temperature is injected using the optimal AR perturbation that leads to the highest injection ratio at KE <500 K—i.e., these contours reflect the best-case capability of a conventional AR perturbation.

antiprotons injected below various KEs is then plotted as a function of initial antiproton number and temperature. (The starting frequency and chirp rate are kept constant at 325 kHz and −120 MHz/s, respectively, to keep the parameter space manageable.)

The self-field of the antiprotons tends to equalize the electric field felt by different parts of the bunch during the perturbation.[15] The fraction of antiprotons that can be excited by the AR perturbation is therefore a function of the density of the bunch,[15] which is, in turn, determined by the initial number and temperature. This explains the drop in the injected fraction on the upper left corner in the plots in Fig. 8: the thermal spreads of these bunches are too great compared with their self-field to remain coherent during the AR perturbation, and some parts of these bunches fail to be excited.

The low-KE injected fraction decreases as the antiproton number increases. This is caused by a mixing of the antiproton's self-field into the KE of the injected antiprotons, due to the electrostatic interaction between the main bulk of the positrons and antiprotons. The overall injected fraction does not decrease since the other antiprotons are injected into the positron plasma at higher KE. This trend means the absolute number of antiprotons injected at low KE increases sublinearly with an increasing initial number of antiprotons.

That the low-KE injected fraction does not significantly improve once the initial antiproton temperature reaches below ∼250 K indicates the spread of the KE distribution of the injected antiprotons is dominated by space charge effects, rather than by the initial temperature, once the latter

is below ∼250 K. The AR injection technique fails to make full use of the low temperatures of the initial bunch.

VII. INCREMENTAL INJECTION

Various schemes to overcome the limitations of AR injection have been investigated using the PPM Vlasov model, and one of these ideas, the so-called incremental injection technique, offers some interesting injection characteristics. This type of scheme has been studied in ALPHA before,[22,23] but under different plasma conditions and with a somewhat different procedure. In this scheme, an antiproton bunch is positioned next to a positron plasma in the configuration shown in Fig. 5. An AR perturbation, with an amplitude of 0.08 V and starting at 325 kHz, is then applied to excite the axial oscillation of the antiproton bunch, but is stopped before injection. The voltage on the AR electrode is subsequently decreased linearly to reduce the voltage separation between the positron and antiproton wells, thereby injecting the already-excited antiproton bunch into the positron plasma. (The rate of the linear ramp is assumed to be slow enough that the positron plasma can redistribute radially through diffusion in case of evaporative escape.) The main tunable parameters in this scheme are the stopping frequency of the AR perturbation and the stopping voltage of the linear ramp. For a fixed stopping frequency, the optimal ramp depth — that which yields the highest injection ratio at KE <10 K, a choice that will be justified later — is determined by running multiple simulations. This optimal ramp depth depends on the stopping frequency, but typically lies within −6 to −7 V. The resultant optimized injection statistics are shown in Fig. 9, for a stopping frequency between
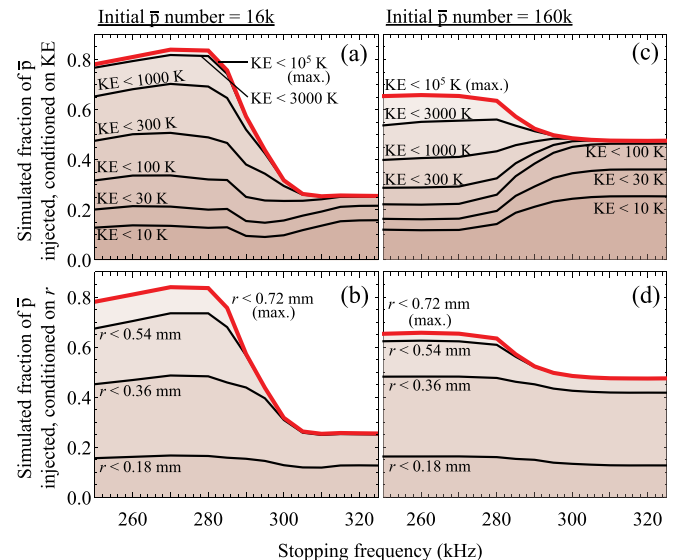

FIG. 9. The simulated, conditional fraction of antiprotons injected into the positron plasma using incremental injection with different stopping frequencies, and two initial antiproton numbers. The rightmost frequency (325 kHz) corresponds to an AR chirp of zero length, with the chirp length increasing towards the left of the horizontal axis. (a) The fraction of antiprotons injected, out of an initial 16 000, conditioned on their KE in the positron plasma. (b) Same as a, except that the ratios are conditioned on radius. (c) The fraction of antiprotons injected, out of an initial 160 000, conditioned on their KE in the positron plasma. (d) Same as c, except that the ratios are conditioned on radius.

250 and 325 kHz (with the upper limit corresponding to a zero-length AR perturbation). The sudden shift in injection behavior at around 290 kHz is expected, since that is where the AR perturbation passes the linear resonance of the antiproton well (297.4 kHz) and starts to excite the antiproton bunch.

From Fig. 9(a), the total (unconditioned) injection fraction of antiproton is observed to increase as a longer AR chirp is used. Figure 9(b) further shows that the increase in the injected fraction comes from improved injection fractions at the outer radii. This can be explained as follows: when only a short chirp is used, the antiprotons reside, more or less, at the bottom of the antiproton well. The antiproton well becomes shallow as the electrode is ramped. However, this decreasing antiproton well depth is not constant across all radial shells. This is *not* due to the fall-off of the vacuum field (the antiproton bunch only has a radius of ~ 0.8 mm, which is much smaller than the 22.3 mm radius of the electrode wall), but rather to the fall-off of the positron self-field. This fall-off causes the outer radial shells to have a higher antiproton well depth than the inner ones (see Fig. 10). When the antiproton well depth at the centre reaches zero (or, more accurately, reaches the level of the thermal spread of the antiprotons), the antiprotons on that shell start to inject, but the outer shells are still confined. Continuing the ramp further will not help inject the outer radii antiprotons. Instead, positrons start to evaporate since the left wall of the positrons (being also the antiproton well) now has a hole at small r. This self-adjusting process of the positrons causes the shape of the antiproton well to remain constant so long as there is still a significant remnant positron population. The AR perturbation helps the antiprotons at the outer radii overcome the residual well by giving them more energy before the linear ramp begins, thereby allowing their injection.

However, Fig. 9(a) shows that this increase in the total injection fraction comes mostly from an increase in the fraction at high KE; the low KE injection fraction actually decreases, indicating a strong broadening in the KE distribution of the injected antiprotons due to the application of the AR perturbation. This broadening becomes more pronounced with more antiprotons (see Fig. 9(c)). Depending on the detailed equilibration and recombination dynamics between positrons and antiprotons, a purely linear ramp without any AR pre-excitation (the rightmost limit in Fig. 9) is eventually going to produce more trappable antihydrogen atoms than a ramp with an AR pre-excitation, as the initial antiproton
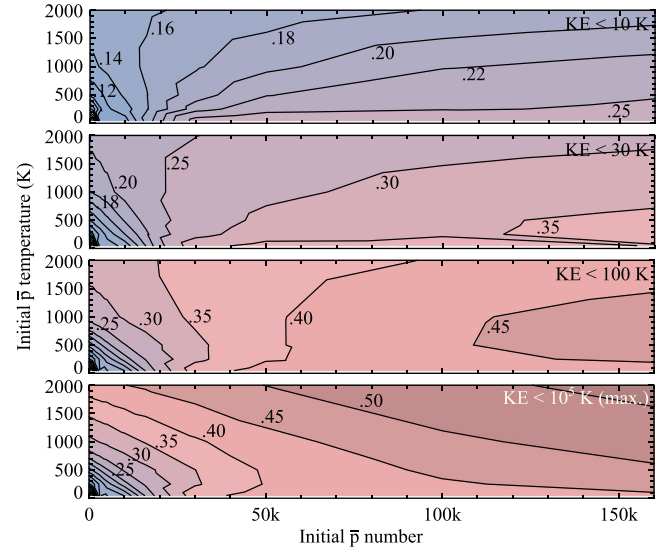
FIG. 11. Contours showing the fraction of antiprotons injected into the positron plasma after a pure linear ramp, against the initial antiproton number and temperature. The four figures show the fraction of antiprotons injected at a KE below the indicated value. Each antiproton bunch with a specific initial number and temperature is injected using the optimal linear ramp depth that leads to the highest injection ratio at KE smaller than 10 K.

number increases. This is possible because the injected fraction at the outer radii increases with antiproton number. The enhanced space charge of the antiproton bunch fills the residual antiproton well at the outer radii and causes the antiprotons on those radii to inject in higher numbers in a pure linear ramp. Using antiproton space charge to overcome the residual well rather than pre-exciting with AR also prevents the KE broadening associated with AR.

Finally, Fig. 11 shows the performance of a pure linear ramp injection (without AR pre-excitation) when applied to antiproton bunches of various initial numbers and temperatures. The final ramp depth for each antiproton bunch is optimized to give the highest injection fraction at KE < 10 K. Table II gives some statistics that compare the AR and the linearly ramp injection scheme under some representative plasma parameters. As argued above, the low-KE injection ratio improves with higher initial antiproton number due to the space charge filling of the residual antiproton well. (However, the converse is also true: low-KE injection performance deteriorates for lower number antiproton bunches. At below ~ 20k antiprotons, the AR injection technique offers a better performance than the pure linear ramp
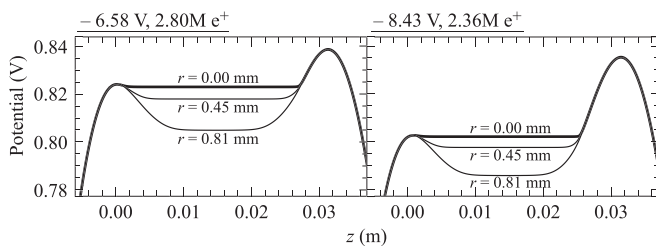

FIG. 10. The external potential seen by the antiprotons during a linear ramp of the AR electrode shown in Fig. 5. The numbers displayed in each subfigure are the electrode's voltage and the number of remaining positrons, the rest being lost to evaporative escape.

TABLE II. Injection performance of some representative plasma parameters, taken from Figs. 8 and 11. The "*Injected, <10 K*" row gives the number of antiprotons injected into the positron plasma at below 10 K. The "*Injected, T fit*" row gives the temperature fit of the KE distribution of injected antiprotons.

	AR injection			Linear injection		
Initial p̄ no.	16 k	160 k	160	16 k	160 k	160 k
Initial p̄ T	250 K	250 K	50 K	250 K	250 K	50 K
Injected, total	11 k	108 k	107 k	4 k	76 k	71 k
Injected, <10 K	1.4 k	2.2 k	9 k	2.7 k	40 k	44 k
Injected, T fit	800 K	2700 K	4500 K	40 K	60 K	40 K

injection.) One can also see from Fig. 11 that the energy distribution of the injected antiprotons is much "colder" than its AR counterpart: there is hardly any difference between the fractions at $KE < 100\,K$ and at $KE < 10^5\,K$. By having fewer fast injected antiprotons, the perturbation on the positron temperature by equilibration is minimized, meaning the perturbation of positrons on the slow injected antiprotons is also minimized. Together with the enhanced number of slow antiprotons, the trappable antihydrogen yield should thus improve significantly. A quantitative prediction of the yield requires an accurate model that reflects the competition between the equilibration and the recombination process, which is currently being investigated.

VIII. CONCLUSIONS AND OUTLOOK

A primary goal of antihydrogen experiments is to gain insight into the bayron asymmetry problem and the validity of CPT symmetry through precision measurements of the physical properties of antihydrogen atoms, including their atomic spectrum, charge neutrality and gravity response. To achieve these measurements, the current state-of-the-art rate of roughly one anti-atom per attempt must be significantly boosted to enhance signal-to-noise ratio, improve statistics, reduce systematics and overcome losses, which is incurred when further cooling trapped antihydrogen atoms to reduce Doppler broadening. A hybrid numerical model has been developed to simulate antiproton and positron dynamics in a nested Penning-Malmberg trap, with the aim of understanding its impact on the yield of trapped antihydrogen atoms. Our model treats the antiproton bunch as a series of concentric shells in which the antiprotons (or, more accurately, their guiding centers) are constrained to move only in the z-direction. The dynamics of antiprotons in each shell is described by a 1D (z, v_z) phase space distribution function which evolves according to the Vlasov equation. The positron plasma is treated quasi-statically in the zero temperature limit as a water bag plasma. Simulation results were in good agreement with experimental measurements on the AR excitation and injection of antiprotons.

The model was used to predict the optimal injection efficiency over a range of initial antiproton numbers and temperatures using the AR injection scheme. It was found that the low-KE injection efficiency deteriorates at high ($\gtrsim 100k$) antiproton numbers and that the efficiency does not improve when low temperature ($\lesssim 250\,K$) antiproton bunches are used due to space-charge effects. This indicates the AR scheme, which proved itself sufficient in earlier experiments, would not scale up well when antiprotons and positrons are mixed in much greater numbers.

An alternative injection scheme, in which antiprotons are injected by a linear lowering of the confining electrostatic potential, was then studied and was seen to offer significant improvement when used in conjunction with intense, low temperature antiproton bunches. These bunches could become available in upcoming experiments and are the focus of much machine and technique development. This work illustrates that existing mixing methods might not exploit new plasma parameter regimes effectively when they become available, but that new, effective methods exist and can be studied numerically. Mixing is not yet a limiting factor in trapping antihydrogen atoms produced from nested Penning-Malmberg traps, and there are good reasons to further develop antiproton accumulation and cooling techniques before more exotic schemes, like antihydrogen atom accumulation and transfer, need be considered.

An in-depth study of the collisional equilibration and recombination between antiproton and positron remains to be done to quantify the number of trapped antihydrogen atoms resulting from various injection techniques, and experiments to realize these techniques are necessary to validate the simulations. The numerical model developed can be used to study other novel injection schemes over a wide range of plasma parameters, and it is applicable to general Penning-Malmberg trap techniques and processes like parallel temperature diagnostics, evaporative cooling and longitudinal separation of like-charged species. New physics can also be incorporated in the numerical model by, for instance, adding Fokker–Planck terms to the Poisson-Vlasov equation to model collisions, or by expanding the phase space dimensionality to include motions in the perpendicular degree of freedom. The restriction on positron quasi-static motion can be relaxed by modeling it with the Vlasov–Poisson–Fokker–Planck equation, though some numerical speed-up is necessary due to time-scale difference.

[1] M. Amoretti, C. Amsler, G. Bonomi, A. Bouchta, P. Bowe, C. Carraro, C. L. Cesar, M. Charlton, M. J. T. Collier, M. Doser, V. Filippini, K. S. Fine, A. Fontana, M. C. Fujiwara, R. Funakoshi, P. Genova, J. S. Hangst, R. S. Hayano, M. H. Holzscheiter, L. V. Jørgensen, V. Lagomarsino, R. Landua, D. Lindelof, E. L. Rizzini, M. Macri, N. Madsen, G. Manuzio, M. Marchesotti, P. Montagna, H. Pruys, C. Regenfus, P. Riedler, J. Rochet, A. Rotondi, G. Rouleau, G. Testera, A. Variola, T. L. Watson, and D. P. van der Werf (ATHENA collaboration), Nature **419**, 456 (2002).

[2] G. Gabrielse, N. S. Bowden, P. Oxley, A. Speck, C. H. Storry, J. N. Tan, M. Wessels, D. Grzonka, W. Oelert, G. Schepers, T. Sefzick, J. Walz, H. Pittner, T. W. Hänsch, and E. A. Hessels (ATRAP collaboration), Phys. Rev. Lett. **89**, 213401 (2002).

[3] G. B. Andresen, M. D. Ashkezari, M. Baquero-Ruiz, W. Bertsche, P. D. Bowe, E. Butler, C. L. Cesar, S. Chapman, M. Charlton, A. Deller, S. Eriksson, J. Fajans, T. Friesen, M. C. Fujiwara, D. R. Gill, A. Gutierrez, J. S. Hangst, W. N. Hardy, M. E. Hayden, A. J. Humphries, R. Hydomako, M. J. Jenkins, S. Jonsell, L. V. Jørgensen, L. Kurchaninov, N. Madsen, S. Menary, P. Nolan, K. Olchanski, A. Olin, A. Povilus, P. Pusa, F. Robicheaux, E. Sarid, S. S. el Nasr, D. M. Silveira, C. So, J. W. Storey, R. I. Thompson, D. P. van der Werf, J. S. Wurtele, and Y. Yamazaki (ALPHA Collaboration), Nature **468**, 673 (2010).

[4] G. Gabrielse, R. Kalra, W. S. Kolthammer, R. McConnell, P. Richerme, D. Grzonka, W. Oelert, T. Sefzick, M. Zielinski, D. W. Fitzakerley, M. C. George, E. A. Hessels, C. H. Storry, M. Weel, A. Müllers, and J. Walz (ATRAP Collaboration), Phys. Rev. Lett. **108**, 113002 (2012).

[5] G. B. Andresen, M. D. Ashkezari, M. Baquero-Ruiz, W. Bertsche, P. D. Bowe, E. Butler, C. L. Cesar, M. Charlton, A. Deller, S. Eriksson, J. Fajans, T. Friesen, M. C. Fujiwara, D. R. Gill, A. Gutierrez, J. S. Hangst, W. N. Hardy, R. S. Hayano, M. E. Hayden, A. J. Humphries, R.

Hydomako, S. Jonsell, S. L. Kemp, L. Kurchaninov, N. Madsen, S. Menary, P. Nolan, K. Olchanski, A. Olin, P. Pusa, C. Rasmussen, F. Robicheaux, E. Sarid, D. M. Silveira, C. So, J. W. Storey, R. I. Thompson, D. P. van der Werf, J. S. Wurtele, and Y. Yamazaki (ALPHA Collaboration), Nat. Phys. **7**, 558 (2011).

[6]C. Amole, M. D. Ashkezari, M. Baquero-Ruiz, W. Bertsche, P. D. Bowe, E. Butler, A. Capra, C. L. Cesar, M. Charlton, A. Deller, P. H. Donnan, S. Eriksson, J. Fajans, T. Friesen, M. C. Fujiwara, D. R. Gill, A. Gutierrez, J. S. Hangst, W. N. Hardy, M. E. Hayden, A. J. Humphries, C. A. Isaac, S. Jonsell, L. Kurchaninov, A. Little, N. Madsen, J. T. K. McKenna, S. Menary, S. C. Napoli, P. Nolan, K. Olchanski, A. Olin, P. Pusa, C. Rasmussen, F. Robicheaux, E. Sarid, C. R. Shields, D. M. Silveira, S. Stracka, C. So, R. I. Thompson, D. P. van der Werf, and J. S. Wurtele (ALPHA Collaboration), Nature **483**, 439 (2012).

[7]S. G. Karshenboim, Phys. Rep. **422**, 1 (2005).

[8]J. H. Malmberg and J. S. deGrassie, Phys. Rev. Lett. **35**, 577 (1975).

[9]F. J. Wysocki, M. Leventhal, A. Passner, and C. M. Surko, Hyperfine Interact. **44**, 185 (1988).

[10]F. Robicheaux, J. Phys. B **41**, 192001 (2008).

[11]G. B. Andresen, M. D. Ashkezari, M. Baquero-Ruiz, W. Bertsche, P. Bowe, C. C. Bray, E. Butler, C. L. Cesar, S. Chapman, M. Charlton, J. Fajans, T. Friesen, M. C. Fujiwara, D. Gill, J. Hangst, W. N. Hardy, R. S. Hayano, M. E. Hayden, A. J. Humphries, R. Hydomako, S. Jonsell, L. V. Jørgensen, L. Kurchaninov, R. Lambo, N. Madsen, S. Menary, P. Nolan, K. Olchanski, A. Olin, A. Povilus, P. Pusa, F. Robicheaux, E. Sarid, S. S. E. Nasr, D. M. Silveira, C. So, J. W. Storey, R. I. Thompson, D. P. van der Werf, D. Wilding, J. S. Wurtele, and Y. Yamazaki (ALPHA Collaboration), Phys. Lett. B **695**, 95 (2011).

[12]G. Andresen, M. Ashkezari, W. Bertsche, P. Bowe, E. Butler, C. Cesar, S. Chapman, M. Charlton, A. Deller, S. Eriksson, J. Fajans, T. Friesen, M. Fujiwara, D. Gill, A. Gutierrez, J. Hangst, W. Hardy, M. Hayden, R. Hayano, A. Humphries, R. Hydomako, S. Jonsell, L. Jørgensen, L. Kurchaninov, N. Madsen, S. Menary, P. Nolan, K. Olchanski, A. Olin, A. Povilus, P. Pusa, E. Sarid, S. S. el Nasr, D. Silveira, C. So, J. Storey, R. Thompson, D. van der Werf, and Y. Yamazaki (ALPHA Collaboration), Nucl. Instrum. Methods A **684**, 73 (2012).

[13]L. Friedland, Scholarpedia **4**, 5473 (2009).

[14]J. Fajans and L. Friedland, Am. J. Phys. **69**, 1096 (2001).

[15]I. Barth, L. Friedland, E. Sarid, and A. G. Shagalov, Phys. Rev. Lett. **103**, 155001 (2009).

[16]G. B. Andresen, M. D. Ashkezari, M. Baquero-Ruiz, W. Bertsche, P. D. Bowe, E. Butler, P. T. Carpenter, C. L. Cesar, S. Chapman, M. Charlton, J. Fajans, T. Friesen, M. C. Fujiwara, D. R. Gill, J. S. Hangst, W. N. Hardy, M. E. Hayden, A. J. Humphries, J. L. Hurt, R. Hydomako, S. Jonsell, N. Madsen, S. Menary, P. Nolan, K. Olchanski, A. Olin, A. Povilus, P. Pusa, F. Robicheaux, E. Sarid, D. M. Silveira, C. So, J. W. Storey, R. I. Thompson, D. P. van der Werf, J. S. Wurtele, and Y. Yamazaki (ALPHA Collaboration), Phys. Rev. Lett. **106**, 025002 (2011).

[17]F. Peinetti, F. Peano, G. Coppa, and J. Wurtele, J. Comput. Phys. **218**, 102 (2006).

[18]E. Fijalkow, Comput. Phys. Commun. **116**, 319 (1999).

[19]P. Colella and P. R. Woodward, J. Comput. Phys. **54**, 174 (1984).

[20]D. L. Eggleston, C. F. Driscoll, B. R. Beck, A. W. Hyatt, and J. H. Malmberg, Phys. Fluids B **4**, 3432 (1992).

[21]L. L. Hurt, P. T. Carpenter, C. L. Taylor, and F. Robicheaux, J. Phys. B **41**, 165206 (2008).

[22]N. Madsen (ALPHA and ATHENA collaboration), AIP Conf. Proc. **862**, 164 (2006).

[23]G. B. Andresen, W. Bertsche, P. D. Bowe, C. Bray, E. Butler, C. L. Cesar, S. Chapman, M. Charlton, J. Fajans, M. C. Fujiwara, D. R. Gill, J. S. Hangst, W. N. Hardy, R. S. Hayano, M. E. Hayden, A. J. Humphries, R. Hydomako, L. V. Jørgensen, S. J. Kerrigan, L. Kurchaninov, R. Lambo, N. Madsen, P. Nolan, K. Olchanski, A. Olin, A. Povilus, P. Pusa, F. Robicheaux, E. Sarid, S. S. E. Nasr, D. M. Silveira, J. W. Storey, R. I. Thompson, D. P. van der Werf, J. S. Wurtele, and Y. Yamazaki (ALPHA collaboration), Phys. Lett. B **685**, 141 (2010).